Naval Research Laboratory
Stennis Space Center, MS 39529-5004

NRL/MR/7174--97-8074

A Simple Acoustic Scattering Model for Ensembles of Rocks and Seashells Lying on the Ocean Floor

CHRISTOPHER FEUILLADE
ROGER W. MEREDITH

Ocean Acoustics Branch
Acoustics Division

MEL D. WAGSTAFF

Planning Systems Incorporated
Slidell, LA 70458

July 24, 1998

REPORT DOCUMENTATION PAGE

Form Approved
OBM No. 0704-0188

1. AGENCY USE ONLY *(Leave blank)*	2. REPORT DATE	3. REPORT TYPE AND DATES COVERED
	July 24, 1998	Final

4. TITLE AND SUBTITLE

A Simple Acoustic Scattering Model for Ensembles of Rocks and Seashells Lying on the Ocean Floor

5. FUNDING NUMBERS

Job Order No. 571686000
Program Element No. 0602435N
Project No.
Task No. UW-35-2-05
Accession No. DN16-3757

6. AUTHOR(S)

Christopher Feuillade, Roger W. Meredith, and Mel D. Wagstaff*

7. PERFORMING ORGANIZATION NAME(S) AND ADDRESS(ES)

Naval Research Laboratory
Acoustics Division
Stennis Space Center, MS 39529-5004

8. PERFORMING ORGANIZATION REPORT NUMBER

NRL/MR/7174--97-8074

9. SPONSORING/MONITORING AGENCY NAME(S) AND ADDRESS(ES)

Office of Naval Research
800 N. Quincy Street
Arlington, VA 22217-5000

10. SPONSORING/MONITORING AGENCY REPORT NUMBER

11. SUPPLEMENTARY NOTES

*Planning Systems Incorporated, 115 Christian Lane, Slidell, LA 70458

12a. DISTRIBUTION/AVAILABILITY STATEMENT

Approved for public release; distribution unlimited

12b. DISTRIBUTION CODE

13. ABSTRACT *(Maximum 200 words)*

This report describes a computer model for predicting levels of acoustic scattering at sonar frequencies from an important class of clutter objects, i.e., rocks and seashells lying on the ocean floor. A simplified modeling approach has been adopted that incorporates basic concepts and principles. Rocks are represented by either grid movable spheres or elastic spheres, a technique that has been previously used to model aqueous suspensions of sand over the equivalent frequency range. Seashells are represented by water-filled spherical shells. The model predicts scattering strength values for areas of the ocean floor covered by ensembles of rocks and shells of sizes, numbers, geologic type, and material compositions typically found in littoral and coastal regions. The results of the model show that ensembles of cobbles and pebbles may give rise to scattering strengths of sufficient magnitude to mask sonar targets or to appear as false sonar targets themselves.

14. SUBJECT TERMS

MCM sonar system designs, high-frequency acoustics, spatial and temporal coherence

15. NUMBER OF PAGES
25

16. PRICE CODE

17. SECURITY CLASSIFICATION OF REPORT	18. SECURITY CLASSIFICATION OF THIS PAGE	19. SECURITY CLASSIFICATION OF ABSTRACT	20. LIMITATION OF ABSTRACT
Unclassified	Unclassified	Unclassified	SAR

A SIMPLE ACOUSTIC SCATTERING MODEL FOR ENSEMBLES OF ROCKS AND SEA-SHELLS LYING ON THE OCEAN FLOOR.

C. Feuillade and R.W. Meredith

Naval Research Laboratory, Stennis Space Center, Mississippi 39529-5004

M.D. Wagstaff

Planning Systems Inc., Slidell, Louisiana 70458

ABSTRACT

This report describes a computer model for predicting levels of acoustic scattering, at sonar frequencies, from an important class of clutter objects, i.e., rocks and sea-shells lying on the ocean floor. A simplified modeling approach has been adopted which incorporates basic concepts and principles. Rocks are represented by either rigid movable spheres or elastic spheres, a technique which has been previously used to model aqueous suspensions of sand over the equivalent frequency range. Sea-shells are represented by water-filled spherical shells. The model predicts scattering strength values for areas of the ocean floor covered by ensembles of rocks and shells of sizes, numbers, geologic type, and material compositions, typically found in littoral and coastal regions. The results of the model show that ensembles of cobbles and pebbles may give rise to scattering strengths of sufficient magnitude to mask sonar targets, or appear as false sonar targets themselves.

INTRODUCTION

Within the last few years, it has been widely recognized that coastal and littoral waters will be the most likely area for future US naval operations. In these regions mines can be used very effectively, and mine warfare, especially the need for improved mine countermeasures (MCM), has become a fundamental concern of the Navy.

A key feature of current Navy requirements is the ability to quickly detect and classify underwater objects, in order to avoid or clear littoral mines. At present, active sonar is the principal means of achieving this objective, due to its capacity for fast, long-range reconnaissance. In shallow-water environments, however, the acoustic response of a target is typically heavily corrupted by reverberant clutter. To optimize sonar operations, therefore, it has become necessary to understand the characteristics of the reverberant acoustic field in order to identify the signatures of targets of interest embedded within it.

Reverberation is due to collective scattering from a large number and diverse range of distributed clutter objects. The different types of obstacle include, for example, bubble clouds and plumes generated at the ocean surface, individual fish and fish schools swimming within the water column, or rocks and sea-shells lying on the bottom. Clearly, it would be intractably difficult, or perhaps impossible, to perform experiments which would isolate and measure the scattering characteristics of all clutter objects. Similarly, the analytical/computational problems associated with providing theoretical target strength estimates of arbitrarily-shaped objects, singly or in ensemble, are widely acknowledged. For these reasons, simplified modeling approaches, which maintain basic physical principles while reducing computational load, and which provide acceptably realistic estimates of scattering strength, hold considerable appeal and are of great utility.

As an application of this modeling rationale, this report describes a model for predicting levels of acoustic scattering from an important class of clutter objects, i.e., rocks and sea-shells lying on the ocean floor. While the model makes a number of simplifying assumptions, it is capable of making determinations for rocks and shells of sizes, numbers, geologic type, and material compositions, typically found in littoral regions. The model leads to some notable results. In particular, it shows that ensembles of cobbles and pebbles may have scattering strengths similar to the target strengths of metal spheres and may also, therefore, mask other targets, or even appear as false sonar targets.

Following this introduction, section 1 of this report describes the modeling approach used to calculate the scattering strength of the sea-floor when covered by rocks and sea-shells. Section 2 develops the theoretical formalism for predicting acoustic scattering from individual and multiple

rigid movable spheres and elastic spheres and shells. In section 3 we apply the formalism to study scattering from rocks and sea-shells of various sizes and compositions. Section 4 gives a brief discussion of some issues raised by the work, and this is followed by a summary of conclusions.

1. MODELING APPROACH

The purpose of the scattering model described in this report is to provide estimates of the scattering strength of ensembles of rocks and sea-shells lying on the sea floor. The approach used to construct the model is depicted schematically in figs.1 and 2. Figure 1 indicates the individual scattering components. Rocks are represented by either rigid movable spheres or elastic spheres. Clearly, rocks are irregular in shape and not generally spherical. A spherical scatterer approximation has been used successfully by Sheng and Hay,[1] however, to obtain reasonable fits to scattering data for aqueous suspensions of sand at frequencies consistent with the requirements of the present application. Sheng and Hay achieved their best fits using the rigid movable sphere representation. They found that the elastic sphere model predicted a resonance structure in the scattered field spectrum which is not observed in the data. The large nonspherical irregularities in shape occurring in real scatterers probably leads to the suppression of such resonance behavior. Sea-shells are represented in the present model (see fig.1) as water-filled spherical shells. While this seems to be a reasonable approach, no data is currently available by which to estimate its validity.

Figure 2 illustrates the method by which the scattering strength of the sea-floor is estimated in the model. Scattering strength is equivalent to target strength per unit area. In the model, a number of spheres or spherical shells of random size and random acoustical properties (i.e., density and, if applicable, elasticity) are randomly placed within an area of 1 square meter. The scattered field from each object is individually calculated, and a coherent sum in the direction of the incident field is then determined. From the aggregate scattered field, the total target strength of the scatterers within the 1 square meter area (and, hence, the scattering strength of the portion of sea floor due to the ensemble) is found. The scattering strength is calculated as a function of the angle of incidence of the incoming field (i.e., the grazing angle). Additionally, in the simulations discussed later in this report, the scattering strength is averaged over a number of "snapshots", i.e., randomizations of geometrical configuration, diameter, density, and other acoustical properties.

Apart from the spherical scatterer approximation itself, the model incorporates four other simplifying assumptions: (a) the sea floor is considered to be acoustically transparent, and therefore does not contribute to the scattering strength; (b) multiple scattering effects between rocks are not included; (c) "shadowing" effects (i.e., the effect of one sphere occluding another) are

neglected, so that all of the scatterers are assumed to experience the same incident field intensity; and (d), none of the rocks are considered to touch each other. The effect of assumptions (a) and (b) should be to reduce scattering strength predictions below what might be expected from experimental measurements; while assumption (c), which is expected to be important only at low grazing angles, should serve to increase scattering strength predictions. Assumption (d) is probably suitable for rocks of cobble and pebble size classes, but may be inappropriate for granules and sea-shells. Overall, it appears safe to regard the model as providing lower bound estimates of scattering strength. Further development is being undertaken to investigate the importance of the underlying assumptions; which should lead to future upgrades of the scattering model by taking their effects into account. Another issue needing examination in the future, which is not considered in the present model, is the effect on scattering strength when rocks are partially buried in the bottom.

2. THEORETICAL DEVELOPMENT

(a) Rigid movable sphere

The theory of scattering from a single rigid immovable sphere was introduced by Anderson.[2] His approach was later modified for a rigid movable sphere by Hickling and Wang.[3] We will consider the case in which a plane wave is incident on a single rigid sphere entrained in water. For simplicity, and with no loss of generality, the positive z-axis is chosen for the direction of incidence. The origin of coordinates is placed at the center of the sphere. The scattering behavior is calculated by expanding the acoustic field in terms of normal modes (i.e., products of Legendre polynomials and spherical Bessel functions) and applying the appropriate boundary conditions at the spherical interface between the media.

The incoming plane wave is described by

$$\phi_I = e^{ikr\cos\theta} = \sum_{m=0}^{\infty} i^m (2m+1) P_m(\cos\theta) j_m(kr) \quad . \tag{1}$$

In this expression (and throughout this development) we suppress the harmonic time dependence $e^{-i\omega t}$, where ω is the frequency of the incident field. The quantity k (= ω/c) is the propagation wavenumber, where c is the sound speed in water. The scattered field is

$$\phi_S = \sum_{m=0}^{\infty} A_m P_m(\cos\theta) h_m(kr) \quad , \tag{2}$$

where the coefficients A_m are to be determined. While the sphere is rigid, it is freely movable under the action of the incoming sound waves. The boundary conditions at the surface r = a of the sphere (a is the radius) are: (i) the normal displacement must be continuous at the surface; (ii) the rate of change of momentum of the sphere is equal to the force exerted by the water as it moves under the action of the incident field. Applying these boundary conditions leads to the following relations:

$$A_m = -i^m (2m+1) \frac{j_m'(ka)}{h_m'(ka)} \qquad (m \neq 1) \, , \tag{3}$$

where: $j_m'(z) \equiv \frac{d}{dz}[j_m(z)]$; $h_m'(z) \equiv \frac{d}{dz}[h_m(z)]$; and

$$A_1 = -3i \frac{\left(\frac{\rho_1}{\rho}\right) ka\ j_1'(ka) - j_1(ka)}{\left(\frac{\rho_1}{\rho}\right) ka\ h_1'(ka) - h_1(ka)} \quad , \tag{4}$$

where (ρ_1/ρ) is the ratio of the density of the sphere to the density of water. The various values of A_m are then incorporated into (2) to determine the scattered field. At scattering distances large relative to ka,

$$h_m(kr) \rightarrow (-i)^{m+1} \frac{e^{ikr}}{kr} \quad . \tag{5}$$

Making substitutions from (3), (4), and (5) into (2) gives, for the backscattered field ($\theta = 180$)

$$\phi_S = \frac{ie^{ikr}}{kr} \left[\left\{ \sum_{\substack{m=0 \\ m \neq 1}}^{\infty} (-1)^m (2m+1) \frac{j_m'(ka)}{h_m'(ka)} \right\} - 3 \frac{\left(\frac{\rho_1}{\rho}\right) ka\ j_1'(ka) - j_1'(ka)}{\left(\frac{\rho_1}{\rho}\right) ka\ h_1'(ka) - h_1'(ka)} \right] , \tag{6}$$

and the corresponding backscattering target strength for a single sphere is:

$$TS = 10 \log_{10} \left[\left| \phi_S (r = 1) \right|^2 \right] , \tag{7}$$

where ϕ_S (r = 1) indicates the backscattered field at a range of 1 meter. If there is an ensemble of N closely spaced scatterers, the total target strength is determined by performing a coherent sum of the backscattered field from the individual spheres, i.e.,

$$TS_E = 10 \log_{10} \left[\left| \sum_{n=1}^{N} \phi_{Sn} (r = 1) \right|^2 \right] . \tag{8}$$

Clearly, in the present application, the value of the coherent sum will be a function of grazing angle, and will exhibit peaks and nulls due to constructive and destructive interference of the scattered fields from the various scatterers.

(b) Elastic sphere

The problem of scattering from an elastic sphere was treated by Faran.[4] The approach is similar to that for the rigid sphere, and the incident and scattered fields are again given by eqs. 1 and 2. However, in this case, an acoustic wave is generated inside the sphere, and this must be

incorporated in the treatment. In the elastic sphere the acoustic displacement $\mathbf{u}_1$ has two components, and is represented in terms of a scalar potential ϕ_1 (the compressional wave component) and a vector potential ψ_1 (the shear wave component) by the equation

$$\mathbf{u}_1 = \text{grad}\,\phi_1 + \text{curl}\,\psi_1 \ , \tag{9}$$

where ϕ_1 and ψ_1 satisfy the equations:

$$\frac{\partial^2 \Phi_1}{\partial t^2} = \left\{ \frac{\lambda_1 + 2\mu_1}{\rho_1} \right\} \nabla^2 \Phi_1 \ ; \tag{10}$$

$$\frac{\partial^2 \Psi_1}{\partial t^2} = \left\{ \frac{\mu_1}{\rho_1} \right\} \nabla^2 \Psi_1 \ . \tag{11}$$

In these equations ρ_1 is again the density of the sphere, and λ_1 and μ_1 are the elastic Lamé constants. Assuming harmonic solutions for (10) and (11), i.e., $\Phi_1 = \phi_1 e^{-i\omega t}$ and $\Psi_1 = \psi_1 e^{-i\omega t}$, yields wavenumbers for compressional propagation (k_L) and shear propagation (k_T) in the elastic medium as follows:

$$k_L = \omega \left(\frac{\rho_1}{\lambda_1 + 2\mu_1} \right)^{\frac{1}{2}} \ ; \tag{12}$$

$$k_T = \omega \left(\frac{\rho_1}{\mu_1} \right)^{\frac{1}{2}} \ . \tag{13}$$

In the elastic sphere the compressional field is expanded

$$\phi_1 = \sum_{m=0}^{\infty} P_m(\cos\theta)\, A_m^1\, j_m(k_L r) \ , \tag{14}$$

and the shear field is

$$\psi_1 = \sum_{m=0}^{\infty} \frac{\partial}{\partial \theta} P_m(\cos\theta)\, C_m^1\, j_m(k_T r) \ . \tag{15}$$

At the interface between the water and the elastic sphere, three boundary conditions are applicable. The normal displacement and normal stress must be continuous, and the tangential stress must be zero. From the continuity of normal displacement we find,

$$\begin{aligned} &(-i)^m (2m+1)\, x\, j_m'(x) + A_m\, x\, h_m'(x) \\ &\quad = A_m^1\, x_L\, j_m'(x_L) - m(m+1)\, C_m^1\, j_m(x_T) \ , \end{aligned} \tag{16}$$

where: $x = ka$; $x_L = k_L a$; and $x_T = k_T a$.

From the continuity of normal stress we find,

$$- \lambda_1 x^2 [(-i)^m (2m + 1) j_m(x) + A_m h_m(x)]$$

$$= x_L^2 A_m^1 [2\mu_1 j_m''(x_L) - \lambda_1 j_m(x_L)] - 2\mu_1 m(m + 1) C_m^1 [x_T j_m'(x_T) - j_m(x_T)] \quad , \qquad (17)$$

and, since the tangential stress must be zero, we have,

$$(m + 2)(m - 1) C_m^1 j_m(x_T) + x_T^2 C_m^1 j_m''(x_T)$$

$$- 2A_m^1 [x_L j_m'(x_L) - j_m(x_L)] = 0 \quad . \qquad (18)$$

Equations 16, 17, and 18 must be solved simultaneously to find A_m. In the computer model here, these equations are solved using Kramer's rule. The quantities A_m are then substituted in (2) to calculate the scattered field. The target strength is again given by (7), and for an ensemble by (8).

(c) Elastic shell

The problem of scattering from an elastic spherical shell was treated by Goodman and Stern.[5] In the shell itself the acoustic displacement $\mathbf{u}_1$ is again given by (9), with ϕ_1 and ψ_1 defined by (10) and (11) etc. In this case the compressional field is expanded

$$\phi_1 = \sum_{m=0}^{\infty} P_m(\cos\theta) \{ A_m^1 j_m(k_L r) + B_m^1 n_m(k_L r) \} \quad , \qquad (19)$$

and the shear field is

$$\psi_1 = \sum_{m=0}^{\infty} \frac{\partial}{\partial\theta} P_m(\cos\theta) \{ C_m^1 j_m(k_T r) + D_m^1 n_m(k_T r) \} \quad . \qquad (20)$$

It is also necessary to define the compressional field within the shell cavity; which in our model is filled with water where sound again propagates with wavenumber k, so that

$$\phi_2 = \sum_{m=0}^{\infty} P_m(\cos\theta) A_m^2 j_m(kr) \quad . \qquad (21)$$

The same three boundary conditions that applied to the elastic sphere, i.e., that the normal displacement and normal stress must be continuous, and that the tangential stress must be zero,

now apply at both the outer and inner boundaries of the shell. From the continuity of normal displacement we find,

$$A_m \, x \, h'_m(x) + (-i)^m \, (2m + 1) \, x \, j'_m(x) = A^1_m \, x_L \, j'_m(x_L) + B^1_m \, x_L \, n'_m(x_L) - m(m + 1) \, C^1_m \, j_m(x_T) - m(m + 1) \, D^1_m \, n_m(x_T) \quad , \quad (22)$$

From the continuity of normal stress we find,

$$\begin{aligned} - \lambda_1 \, x^2 \, [(-i)^m \, (2m + 1) \, j_m(x) + A_m \, h_m(x)] = & - \lambda_2 \, x_L^2 \, \{A^1_m \, j_m(x_L) + B^1_m \, n_m(x_L)\} \\ & + 2\mu_2 \, x_L^2 \{A^1_m \, j''_m(x_L) + B^1_m \, n''_m(x_L)\} \\ & + 2m(m + 1) \, \mu_2 \, C^1_m \, \{ \, j_m(x_T) - x_T \, j'_m(x_T) \, \} \\ & + 2m(m + 1) \, \mu_2 \, D^1_m \, \{ \, n_m(x_T) - x_T \, n'_m(x_T) \, \} \quad , \quad (23) \end{aligned}$$

and finally, since the tangential stress must be zero, we find

$$\begin{aligned} & -2 \, A^1_m \{x_L \, j'_m(x_L) - j_m(x_L)\} - 2 \, B^1_m \{x_L \, n'_m(x_L) - n_m(x_L)\} \\ & + C^1_m \, \{(m + 2)(m - 1) \, j_m(x_T) + x_T^2 \, j''_m(x_T) \, \} \\ & + D^1_m \, \{(m + 2)(m - 1) \, n_m(x_T) + x_T^2 \, n''_m(x_T) \, \} = 0 \quad . \quad (24) \end{aligned}$$

As described by Goodman and Stern,[5] a corresponding set of equations (with variables $y = ka'$, $y_L = k_L a'$, and $y_T = k_T a'$; where a' is the *inner* radius of the shell) is obtained when these boundary conditions are applied at the inner shell surface.

In all, six equations are obtained by applying the boundary conditions at the interfaces. In the monopole (m=0) case, the number of equations is four. Goodman and Stern describe a method of tabulating the equations in matrix form, and then solving for A_m using Kramer's rule. The quantities A_m are then substituted in (2) to calculate the scattered field. The target strength is given by (7), and for an ensemble by (8).

The method of using Kramer's rule to determine A_m, for the elastic sphere and elastic shell cases, is a convenient and accurate procedure for investigating the scattering behavior, and has been adopted for the model described in this report. Calculating the elements of the matrix and evaluating the determinant are readily vectorizable operations, and an efficient algorithm has been implemented in MATLAB.

3. APPLICATION TO SCATTERING FROM ROCKS AND SEA-SHELLS

TYPICAL SIZES OF ROCKS AND SEA-SHELLS

Six geologic rock types were modeled using the rigid and elastic sphere scattering models. In addition, one type of sea-shell was modeled with both the elastic shell and elastic sphere scattering models. The sizes of the objects used in the various models were selected based on the diameter classification system shown in Table 1.[6] Ensembles of cobbles, pebbles, granules, and sea-shells were modeled separately. The mean and standard deviation of the diameter for each scatterer type were used to select a diameter for each object via a randomizing algorithm.

Table 1. Udden-Wentworth diameter classification

Rock/shell type:	cobbles	pebbles	granules	sea-shells
Diameter (mm)	$32 \rightarrow 256$	$4 \rightarrow 32$	$2 \rightarrow 4$	$4 \rightarrow 128$
Diameter (ϕ)	$-5 \rightarrow -8$	$-2 \rightarrow -5$	$-1 \rightarrow -2$	$-2 \rightarrow -7$
Mean (mm)	144	18	3	66
St. Dev. σ (mm)	158	20	1.4	87.7

The ϕ values listed in Table 1 represent a logarithmic method for denoting grain and rock sizes, commonly used in geological work. These quantities are defined by $2^{-\phi}$ = diameter (mm). The elastic properties of the six different rock types, and the one shell type, are listed in Table 2. The elastic values were deduced from several references,[6-14] not all of which agree completely.

Table 2. Scatterer types and elastic properties used in modeling

Type		ρ (g/cc)	Std. Dev. (g/cc)	c_L (m/s)	Std. Dev. (m/s)	c_T (m/s)	Std. Dev. (m/s)
Sedimentary							
1	Sandstone	2.35	0.8	2850	500	1602	310
2	Shale	2.4	1.0	2725	813	1507	525
3	Limestone	2.55	0.7	2950	2295	1673	1358
4	Dolomite	2.7	0.4	5200	2404	2953	1410
	Average	2.5	0.74	3431	1503	1949	1078
5 Igneous		2.82	0.34	5755	600	3265	329
6 Metamorphic		2.81	0.25	5140	458	2915	255
7 Sea-shells		2.65	0.05	6566	260	3414	140

Sea-shells were modeled three times: twice as spheres, using both the elastic sphere model and the rigid movable sphere model; and once as fluid- (i.e., water-) filled shells, using the elastic shell model. Using the shell model, the sea-shell thickness was maintained at a constant value of 3mm.

Due to lack of data, the standard deviations of the compressional and shear velocities for shells were determined in an unusual way, i.e., they were derived by assuming that the ratio of the standard deviation of the density to the standard deviation of the velocity for shells would be the same as exhibited by the other rock types.

MODELING RESULTS

All scattering strength calculations were performed at a frequency of 35kHz. In all of the modeling performed for this study, no statistical dependence on the grazing angle was observed. Also, no significant deviation from a Gaussian distribution was observed in the scattering strength.

(a) Scattering from rocks

Figure 3, which was derived using the elastic sphere scattering model, shows the modeled scattering strength for the three rock size classes (i.e., cobbles, pebbles, and granules) shown in Table I, and for the six rock types defined in Table II. Sea-shells are treated separately. For a given size class and rock type, each datum point represents the mean value of the scattering strength of one ensemble sample, averaged over grazing angles. For each ensemble sample, the diameters of the individual scatterers, their compressional and shear sound speeds, and their densities, were randomly selected by assuming a Gaussian distribution bounded within the ranges specified for each parameter by Tables 1 and 2. A variation over the object number density (i.e., number of scatterers within a square meter) was also incorporated. For cobbles, samples with 4, 5, 6, 7, 8, and 9 scatterers per square meter were plotted together. With these values, the surface area of the bottom covered by scatterers varied between about 20% and 40%. For pebbles, samples with 600, 700, 800, 900, 1000, 1100, 1200, and 1500 scatterers per square meter were plotted together. With these values, the surface area of the bottom covered by scatterers varied between about 40% and 100%. For granules, samples with 1000, 2500, 5000, and 1-8 ($x10^4$) scatterers per square meter were plotted together. This gave a coverage of the surface area of the bottom which varied between about 1% and 80%.

Inspection of figure 3 shows that the scattering strength varies widely, and depends strongly on both the rock type and the rock size class. For cobbles, the scattering strength varies between -1dB (dolomite - rock type 4) and -31dB (igneous - rock type 5). For pebbles, the scattering strength varies between about -3dB (sandstone) and -16dB (igneous). For granules, the scattering strength varies between about -19dB (shale - rock type 2) and -52dB (metamorphic). For a given rock size, igneous and metamorphic rocks (types 5 and 6) typically show a lower scattering strength than the other rock types (i.e., about 7-11 dB lower for cobbles, 4-7 dB lower for pebbles, and about 3 dB

lower for granules). This behavior is due to the differing elastic properties of the various materials used to represent the rocks. Also notable are wide ranges in the predicted scattering strength, particularly for cobble sized rocks (e.g., ~26dB for dolomite - rock type 4) and granules (e.g., ~29dB for metamorphic rocks - type 4). These wide ranges are probably due to the highly variable resonance structure of elastic spheres. As suggested by Sheng and Hay, it is likely that such resonances are suppressed in real rocks, due to the naturally large variation and nonuniformity of their shapes. As we shall see below, both the scattering strength variation with rock type, and the wide scattering strength ranges, largely disappear when the rigid movable sphere scattering model is used instead of the elastic sphere model.

Figure 4, which was also derived using the elastic sphere scattering model, shows the dependence of the scattering strength on the object number density, rather than rock type. Again, the modeled scattering strength for the three rock size classes given in Table 1 is displayed. In this case, for a given size class and number density, each datum point represents the mean value of the scattering strength of an ensemble sample, averaged over grazing angles and over the six rock types.

In the case of cobbles, we see that the scattering strength shows an increase as a function of the number density of scatterers, but that this tends to be overwhelmed by the variability, or spread, due to the variation of elastic parameters. Pebbles, however, indicate a reduced and much more uniform spread of values. In this case the model clearly indicates a moderate increase in scattering strength as the number of pebble scatterers increases [~log (density)]. Granules also exhibit a reduced spread of values. Again, the increase in the scattering strength with the number density of scatterers [~ log(density)] is very apparent.

Figure 5 shows scattering strengths for the three rock size classes given in Table 1, and for the six rock types defined in Table II, but modeled using the rigid movable sphere scattering model, rather than the elastic sphere model. As in figure 3, each datum point represents the mean value of the scattering strength of one ensemble sample, averaged over grazing angles. In this case, for each ensemble sample, only the diameters of the individual scatterers and their densities were randomly selected (elastic properties, i.e., compressional and shear sound speeds, are not incorporated in the rigid sphere model). Again, as in figure 3, scattering strength values for various object number densities are plotted together. For cobbles, samples with 4, 5, 6, 7, 8, 9, and 10 scatterers per square meter were plotted together. For pebbles, samples with 600, 700, 800, 900, 1000, 1100, 1200, and 1500 scatterers per square meter were plotted together. For granules, samples with 1000, 2500, 5000, and 2-8 ($x10^4$) scatterers per square meter were plotted together. The percentages of the bottom surface area covered in each case were similar to the equivalent elastic sphere modeling cases.

When figure 5 is compared with figure 3, one feature that is immediately noticeable (and is quite apparent for all three rock size classes), is the uniformity of the scattering strength as a function of rock type (averaging about -19 dB for cobbles, -15 dB for pebbles, and -34dB for granules). Since the different rock types are represented only by their density parameters in the rigid movable sphere model, this implies that the variations in scattering strength with rock type seen in figure 3, but noticeably absent from figure 5, must be due primarily to changes in the elastic parameters, rather than the densities. Further comparison of figures 3 and 5 also shows that, for most combinations of rock size class and rock type, the rigid movable sphere model typically leads to a lower average scattering strength than the elastic sphere model (e.g., the average scattering strength for sandstone cobbles is reduced by about 12dB). Also, for cobbles, the spread of scattering strength values for each rock type is apparently reduced by using the rigid movable sphere model rather than the elastic sphere model, but this effect is not seen for the pebble and granule size classes.

Figure 6 shows scattering strengths for the three rock size classes given in Table 1, plotted as a function of the object number density. Again these data were modeled using the rigid movable sphere scattering model, rather than the elastic sphere model. As in figure 4, for a given size class and number density, each datum point represents the mean value of the scattering strength of one ensemble sample, averaged over grazing angles and over rock types. However, only the diameters of the individual scatterers and their densities were randomly varied since, as stated above, elastic properties are not incorporated in the rigid sphere model. Immediately noticeable in this case is a reduced spread in scattering strength values for all three rock size classes. Cobbles still show the greatest variability, but now a rising trend in the scattering strength values as a function of number density may be discerned. The [log(density)] variation in scattering strength is also apparent for pebbles and granules.

Since the only substantive difference in the calculations used to obtain the data for figure 6 (as compared with figure 4) is the omission of elastic effects in the sphere, the greater scattering strength variability exhibited in figure 4 must be due to the action of these effects, and to the concomitant changes in scattering resulting from the frequency dependent resonance behavior of the elastic sphere. If the argument of Sheng and Hay[1] is correct (i.e., that the elastic sphere model predicts a resonance structure in the scattered field which, due to irregularities in shape of the individual scatterers, is not observed in the data) then, in the present case, we should take the predictions of the rigid movable sphere model as giving a more realistic indication of the scattering behavior of rocks on the sea floor.

(b) Scattering from sea-shells

Figure 7 shows scattering strength values for sea-shells as a function of number density, modeled using three approaches: (a) treating them as uniform elastic spheres with acoustic and density parameters equivalent to those of the sea-shell carapace; (b) treating them as uniform movable rigid spheres with density parameters equivalent to those of the carapace; (c) treating them as elastic spherical shells (whose acoustic and density parameters are those of the shell carapace) filled with sea-water. The values for sea-shells modeled as elastic spheres are denoted by the symbol "o" ; the values for sea-shells modeled as rigid spheres are denoted by "+" ; and the values obtained using the water-filled elastic shell approach are denoted by "*". The diameter of the sea-shells was varied between 4 and 128mm. Figure 7 clearly shows that the scattering strength of sea-shells, modeled using all three approaches, displays the expected [log(density)] behavior. For most of the number density cases, the scattering strength predicted using the elastic sphere model shows a wider range of values than the rigid model (as previous results would lead us to expect). Interestingly, the scattering strength of sea-shells modeled as water-filled elastic shells is comparable to the values obtained with the elastic sphere model and, for some of the number density cases, has a median value which is 1-2 dB higher. The scattering strength of the water-filled shells is also, of course, dependent upon the thickness of the shells. For the cases shown in figure 7, the shell thickness was maintaiuned at a constant value of 3mm. When the thickness is reduced, the scattering strength falls. Figure 8 shows the scattering strength as a function of number density for thick and thin shells. The points labeled "o" indicate the scattering strength, averaged over a series of ensembles, for number densities 5, 10, and 14 scatterers per square meter, for shells of thickness between 0.3 - 3.8mm (as in figure 7). The points labeled "+" indicate the corresponding scattering strengths, for the same number densities, for shells whose thickness was allowed to vary randomly and uniformly between 0.3 - 1.3mm. We see that the reduction in shell thickness causes the scattering strength to fall by about 5-6dB.

(c) Scattering from single large objects

As a reference for the ensemble model results, we show in Table 3 target strength values for a single spherical scatterer of diameter 0.9 m, and several different elastic properties.

Table 3. Single Sphere Target Strengths

Metal Type	ρ (g/cc)	c_P (m/s)	c_T (m/s)	Target Strength (dB) (elastic model)	Target Strength (dB) (rigid model)
Steel	7.8	5790	3100	-11.1	-13.0
Aluminum	2.7	6420	3040	-19.4	-12.9
Brass	8.7	4700	2110	-9.8	-13.0
Glass	2.32	5640	3280	-9.8	-12.9

Comparison of Table 3 with figs. 3 and 4 indicates that ensembles of cobbles and pebbles, modeled as elastic spheres, may give rise to scattering strengths similar to the target strengths of metal spheres of diameter 0.9m. When the rigid model is used (see figs. 5 and 6), cobbles and pebbles give rise to scattering strengths about the same as the target strength of an aluminum sphere of this diameter. The scattering strengths of granules and low number density sea-shells (see figs. 7 and 8) are smaller than the target strengths of the reference spheres.

CONCLUSIONS

A model for predicting the sonar scattering strengths of ensembles of rocks and sea-shells lying on the ocean floor has been presented. While a simplified modeling approach has been adopted, the model is capable of making realistic determinations for rocks and shells of the sizes, numbers, geologic type, and material compositions, typically found in littoral regions. The results of the model show that ensembles of cobbles and pebbles may give rise to scattering strengths of sufficient magnitude to mask sonar targets, or appear as false sonar targets themselves.

Clearly, the theoretical results presented in this report require experimental verification. Some simple investigations could be undertaken to determine whether the elastic or rigid model leads to more realistic predictions of target strength, and whether surface roughness makes a measurable difference. For example, a number of experiments could be performed using glass marbles (glass has elastic properties similar to rock) and the NRL target cage, and spanning a predetermined range of frequencies and cage orientations. The marbles could be deployed and recovered by divers. A first trial would be with the empty target cage over an undisturbed sand bottom. The second would be over a sand bottom covered with smooth glass marbles. A third trial could be over an undisturbed sand bottom covered with the same marbles that have been sand blasted (so that the glass surfaces are rough and pitted), and possibly also broken into pieces. The same sequence of trials could be performed over a bare sand bottom that has been manually smoothed.

ACKNOWLEDGMENT

This work was funded by the Office of Naval Research, Program Element 62435N, with technical management provided by the Naval Research Laboratory via the High Resolution MCM Environmental Acoustics Clutter Project.

REFERENCES

1 J. Sheng and A.E. Hay, "An examination of the spherical scatterer approximation in aqueous suspensions of sand," J. Acoust. Soc. Am. **83**, 598-610 (1988).

2 V.C. Anderson, "Sound scattering from a fluid sphere," J. Acoust. Soc. Am., **22**, 426-431 (1950).

3 R. Hickling and N.M. Wang, "Scattering of sound by a rigid movable sphere," J. Acoust. Soc. Am. **39**, 276-279 (1966).

4 J.J. Faran, Jr., "Sound scattering by solid cylinders and spheres," J. Acoust. Soc. Am. **23**, 405-418 (1951).

5 R.R. Goodman and R. Stern, "Reflection and transmission of sound by elastic spherical shells," J. Acoust. Soc. Am., **34**, 338-344 (1962).

6 M.R. Leeder, *Sedimentology,* (George Allen and Unwin, London, 1982) pp. 35-37.

7 E.L. Hamilton, "Variations of density and porosity with depth in deep sea sediments," Journal of Sedimentary Petrology, **46**(2), 280-300 (1976).

8 S.P. Clark, *Handbook of Physical Constants,* (Geological Society of America, New York, 1976) pp. 20, 26, 160-168, 197-204.

9 M.B. Dobrin, *Introduction to Geophysical Prospecting,* (McGraw-Hill, New York, 1976) pp. 48-53, 455-460.

10 R.S. Carmichael, *Handbook of Physical Properties of Rocks, Volume III,* (CRC Press, Boca Raton, FL, 1984) pp. 1-38.

11 G. Shumway, "Sound speed and absorption studies of marine sediments by a resonance method", Geophysics, **25**(2), 451-467 (1960).

12 E.L. Hamilton, "V_p/V_s and Poisson's ratios in marine sediments and rocks", J. Acoust. Soc. Am. **66**, 1093-1101 (1979).

13 *A Physicist's Desk Reference,* edited by H.L. Anderson (American Institute of Physics, New York, 1989) p. 56.

14 W. M. Telford, L.P. Geldart, and R.E. Sheriff, *Applied Geophysics,* (Cambridge University Press, New York, 1990) p. 74.

FIGURE 1

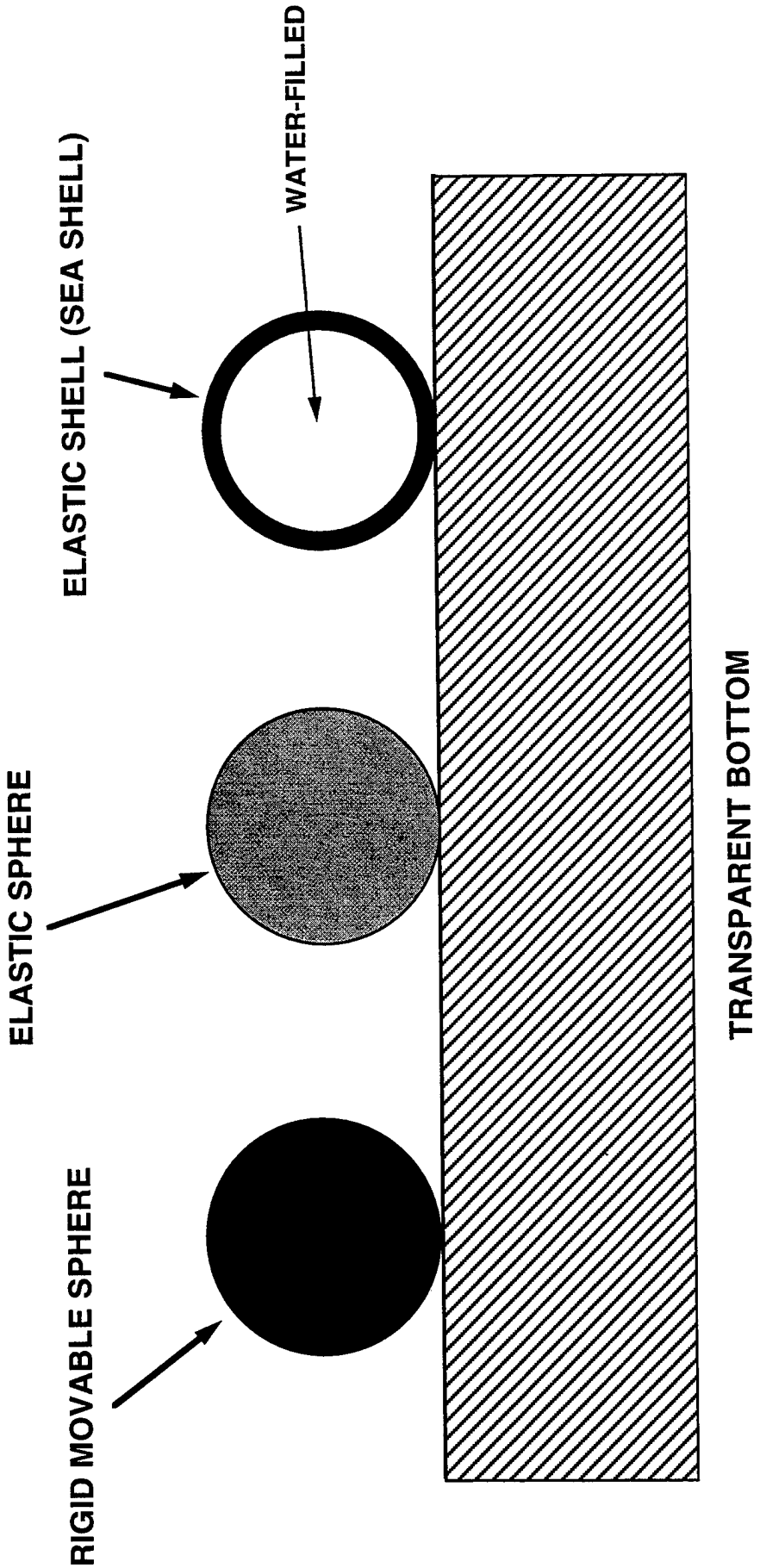
WATER-FILLED
ELASTIC SHELL (SEA SHELL)
ELASTIC SPHERE
RIGID MOVABLE SPHERE
TRANSPARENT BOTTOM

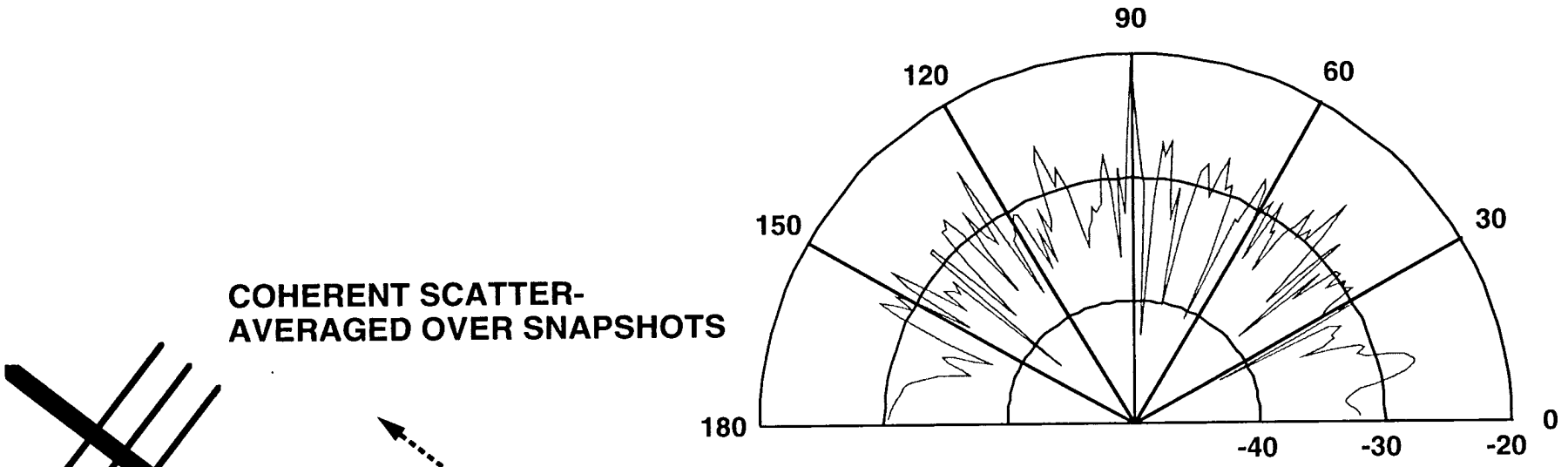

SCATTERING STRENGTH (dB) AS FUNCTION OF GRAZING ANGLE

COHERENT SCATTER-
AVERAGED OVER SNAPSHOTS

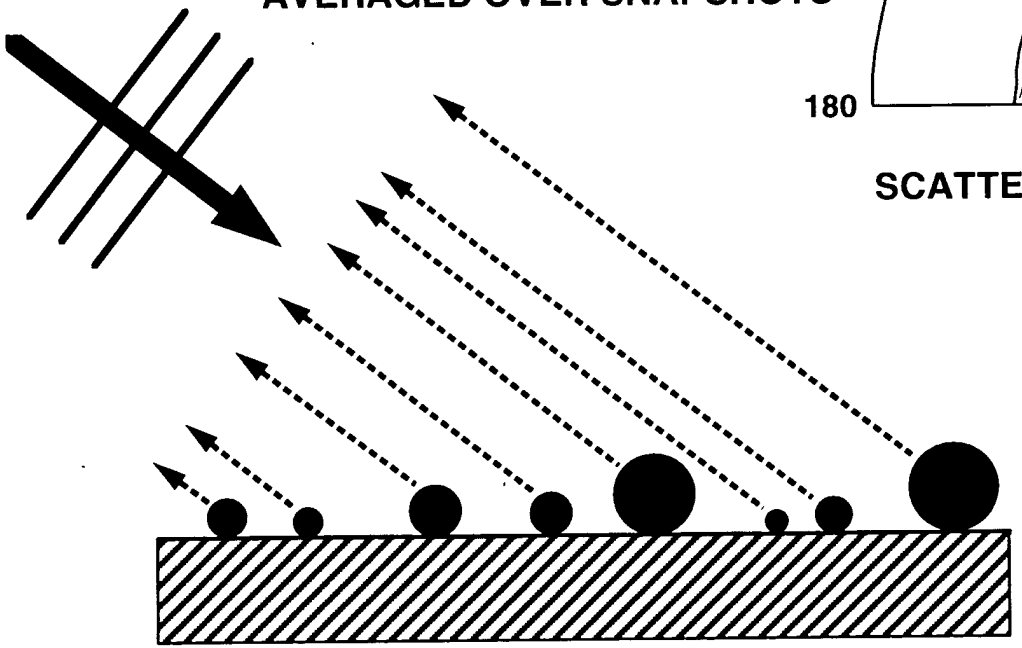

TRANSPARENT BOTTOM

RIGID MOVABLE SPHERES
ELASTIC SPHERES/SHELLS

RANDOMIZE RADIUS

RANDOMIZE LOCATIONS

RANDOMIZE DENSITY

RANDOMIZE ACOUSTIC PARAMETERS

FIGURE 2

Elastic model scattering strength as a function of rock type

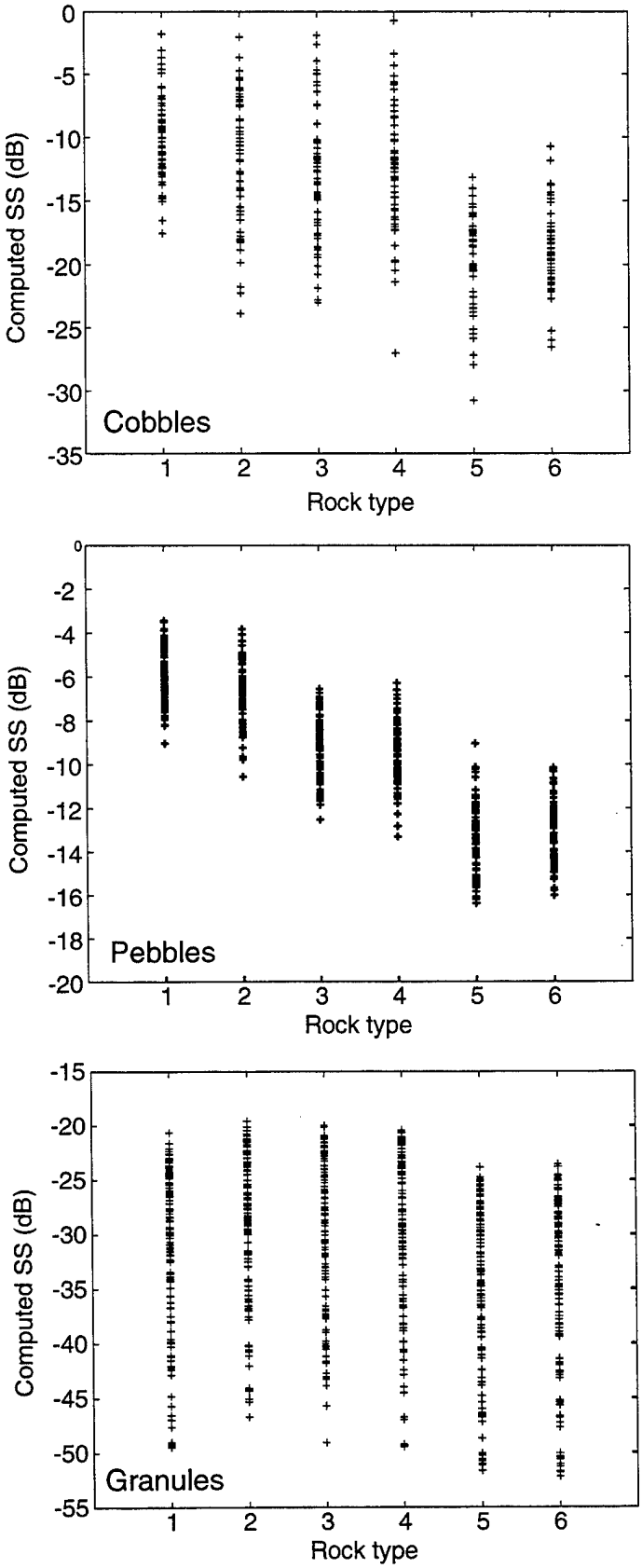

FIGURE 3

Elastic model scattering strength as a function of object density

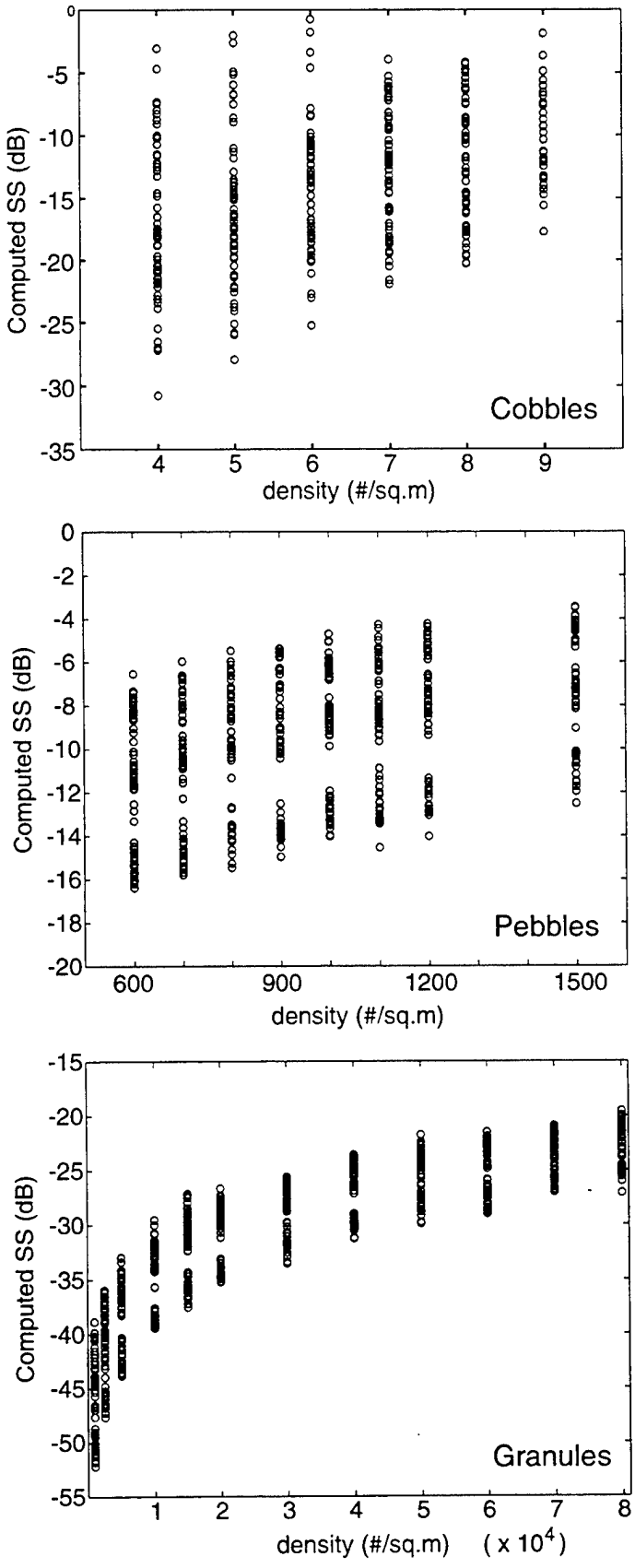

FIGURE 4

Rigid model scattering strength as a function of rock type

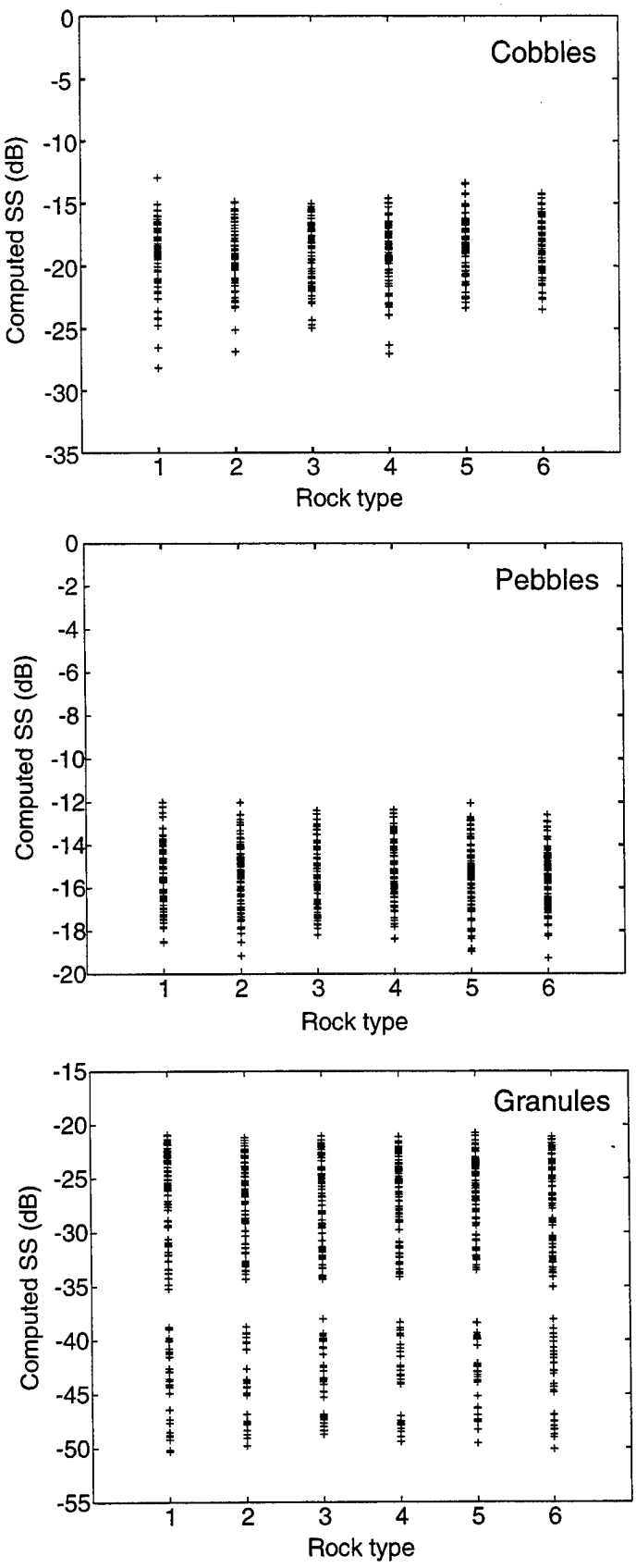

FIGURE 5

Rigid model scattering strength as a function of object density

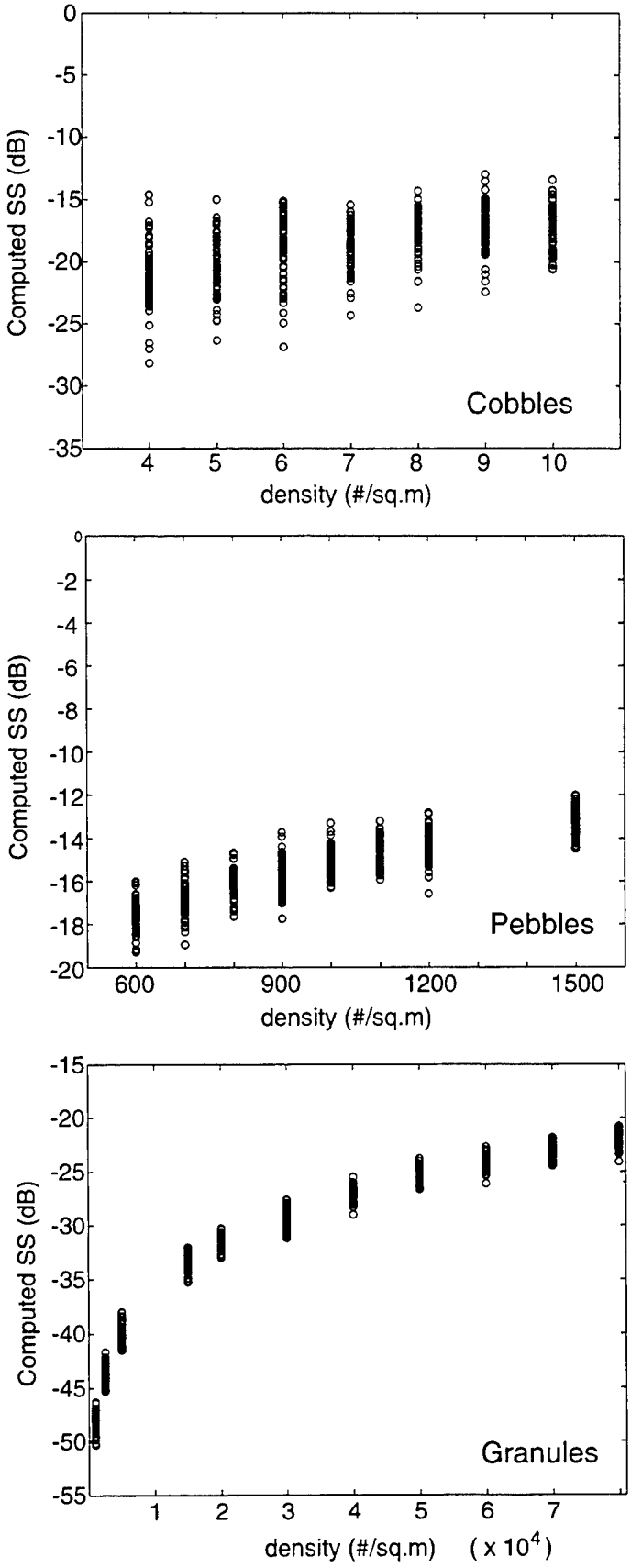

FIGURE 6

FIGURE 7

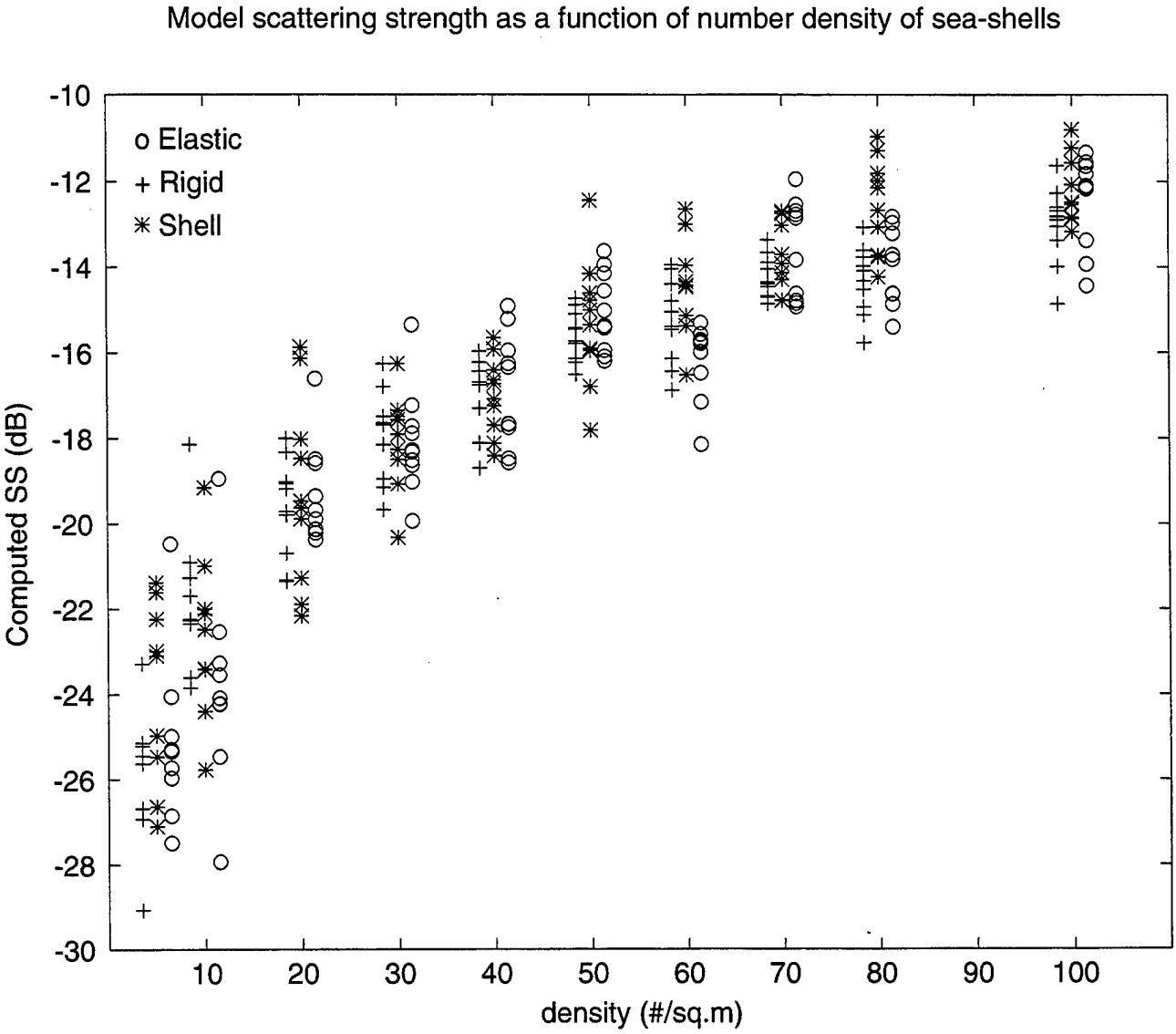
Model scattering strength as a function of number density of sea-shells
o Elastic
+ Rigid
* Shell
Computed SS (dB)
-10
-12
-14
-16
-18
-20
-22
-24
-26
-28
-30
10
20
30
40
50
60
70
80
90
100
density (#/sq.m)

FIGURE 8

Shell model scattering strength as a function of object density for thin and thick shells.